Nanofibrillated Cellulose–Regolith Composite Aerogels for Lunar Thermal Insulation

Jacob Staker[1], Janice Mather[2], Annabelle Hegeman[2], Daniel A. Scheiman[3], Jamesa L. Stokes[4], Andres Tovar[5], Haiquan Guo[,3], Alexander Wei*[,1,6]*

[1]James and Margaret Tarpo Department of Chemistry, Purdue University, West Lafayette, IN 47907, USA

[2]University of Akron, Akron, OH 44325, USA

[3]Universities Space Research Association, Cleveland, OH 44135, USA

[4]NASA Glenn Research Center, Cleveland, OH 44135, USA

[5]School of Mechanical Engineering, Purdue University, Indianapolis, IN 46202, USA

[6]School of Materials Engineering, Purdue University, West Lafayette, IN 47907, USA

*Authors to whom correspondence should be addressed.

KEYWORDS: Aerogel, Cellulose, Composites, Green Chemistry, In-Situ Resource Utilization (ISRU), Regolith, Thermal Management

ABSTRACT

Life support systems in extraterrestrial settings face severe material constraints, demanding innovative in situ resource utilization (ISRU) strategies. One material that merits attention is cellulose, which can be procured in relative abundance from locally generated waste. Here we present an ISRU approach toward thermally insulating composite aerogels based on nanofibrillated cellulose (NFC) and a lunar regolith simulant. Recycled cellulose fibers are ground by planetary ball milling with lunar highland simulant (LHS-1) into NFC–regolith slurries with subsequent conversion into aerogels by supercritical drying. Comminution of cellulose fibers and LHS-1 particles enable the production of composite aerogels with thermal conductivities as low as 30 mW/m·K. Multi-parametric optimization of aerogel properties can be guided by design of experiments (DOE) based on the mass ratios of NFC in water, LHS-1 in aerogel, and amount of milling media. The study illustrates how composite aerogels made of regolith and fibrillated cellulose can provide sustainable routes toward functional materials for lunar habitats and other extraterrestrial resource-limited environments.

INTRODUCTION

Cellulose, the most abundant biodegradable polymer on Earth [1], is commonly sourced from woody plants and agricultural biomass [2,3]. Cellulose can also be extracted from various waste streams and repurposed as second-generation feedstocks [4]; those with high cellulose content can be dispersed readily into cellulose microfibers (CMF), and further chemo-mechanical treatments can be applied with relatively low energy and mild chemistries to generate cellulose nanofibers and nanocrystals [5]. The recent rise in popularity of nanocellulose stems from its high surface area and ability to impart composite materials with mechanical strength in ways not achievable in microfiber form [6]. In particular, mechanochemical processes are a scalable and sustainable approach for fibrillation of CMF to submicron dimensions, with efficiency depending on mill type, grinding media, energy input, and use of additives [7,8]. Planetary mills with milling media [9] operate at high angular speeds and can be efficient at generating Coriolis and shear forces [10,11,12], which is expected to enable comminution in low-gravity environments.

Extraterrestrial cellulose is far from ubiquitous, however it is remarkably abundant in human-generated waste products during space missions: for example, wastepaper is 60–70% cellulose by weight [13], whereas cotton fabrics can contain up to 99% [14,15]. A logistical model developed for crewed missions lists ten categories of waste with at least half containing cellulose including paper, packaging, clothing, and hygiene products [16]. Waste reduction is an important priority in space-related missions and future lunar habitations: the U.S. National Aeronautics and Space Administration (NASA) has projected waste management as a major issue in long-distance expeditions such as the Gateway and Artemis missions and for longer-term goals of extraterrestrial settlement [17]. Thus, the upcycling of cellulose-rich waste in such settings offers the dual benefit of recovering precious imported resources while reducing waste volume.

The valorization of cellulose can be increased further when blended with locally sourced materials into composites with a gain in function, a key aspect of in situ resource utilization (ISRU) [18,19]. In particular, the compressive strength of lunar regolith, the base material for geopolymer matrices in lunar construction [20,21,22,23,24], can be enhanced by adding upcycled biopolymers as binding agents [25,26,27,28]. Mixtures of regolith and biopolymers have been freeze-dried into insulative aerogels as an ISRU approach to thermal management, with bulk densities and thermal conductivities as low as 0.34 g/cm^3 and 70 mW/m·K having been reported [29]. Regolith reinforced with micro- or nanofibrillated cellulose (MFC or NFC) has obvious appeal for such objectives, but to the best of our knowledge this approach has yet to be explored; discussions on cellulose-based feedstocks in space so far have focused on microbial biodegradation and bioregeneration [30,31]. We note that MFC and NFC both describe cellulose that has been fibrillated to submicron dimensions [6,34], and refer to the latter due to its popular usage.

In this study, we use mineral-assisted milling of cellulose pulp with Lunar Highlands Simulant (LHS-1) to create NFC-reinforced aerogels with potential utility for thermal insulation. LHS-1 is a terrestrial, Ca-rich aluminosilicate (plagioclase) with smaller amounts of silicate glass and metal oxides (Fe and Ti), representing one of several regolith species ubiquitous to the lunar environment. The materials qualities of regolith-based composites are largely untapped and thus offer ample opportunity for discovery and development. Wet milling of LHS-1 and cellulose generates slurries of ultrafine materials that can be converted upon supercritical drying (SCD) into composite aerogels with thermal conductivities as low as 30.9 mW/m·K. A multifactorial design-of-experiments (DOE) approach can also be used to optimize the mass ratios of NFC (w/w% in slurry), LHS-1 (wt% in aerogel), and number of milling media for thermal insulation with ISRU constraints or any combination of physical properties.

EXPERIMENTAL SECTION

Materials. Cellulose microfibers (CMF) were derived from research-quality filter paper (Whatman Grade 1) with low ash content (Cytiva, Marlborough, MA) shredded in a food blender. These cellulose fibers are reported to have a crystallinity index of 0.71 [57]. LHS-1 (median particle size 80 μm) was acquired from Space Resource Technologies (Oviedo, FL). Milling media comprised of yttria-stabilized zirconia (YSZ) were obtained as 1-cm cylinders, 1-cm spheres, or 1-mm spheres from MSE Supplies (Tucson, AZ). *Tert*-butyl alcohol (TBA) was acquired from Thermo Fisher Scientific (Waltham, MA), and deionized water was obtained using a Milli-Q ultrafiltration system from MilliporeSigma (Burlington, MA) with a measured resistivity above 18 MΩ·cm and passed through a 0.22-μm filter.

Ball Milling of Cellulose and LHS-1. Mixtures of shredded filter paper and LHS-1 were dispersed in deionized water with YSZ milling media in a nylon or polycarbonate (Nalgene) bottle placed on various milling equipment: planetary milling was performed using a MSK-SFM-3 mill (MTI, Richmond, CA) operating at 25 Hz (60 *g*) or a Pulverisette 7 mill operating at 10 Hz (63 *g*), whereas rotary milling was performed using a custom-built tumbler operating at 400 rpm. Formulations were prepared with consistent amounts of NFC and LHS-1 (25%, 50%, and 75% mass ratios) and dispersed in deionized water to a final mass of 50 g, then milled with varying amounts of YSZ media for 2 hours (**Figure 1**). The NFC/LHS-1 slurries were either separated by three rounds of centrifugation and redispersion in fresh water for further characterization or converted directly into composite aerogels (see below).

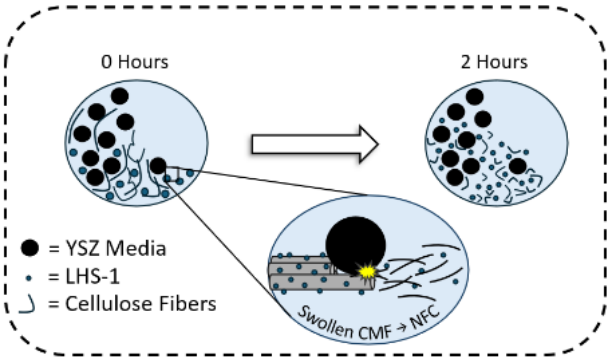


Figure 1. Mineral-assisted wet milling of cellulose microfibers (CMF) into NFC.

Fiber Width Distribution Analysis. Analytical NFC samples were prepared by treating an aqueous aliquot with sufficient TBA to form a 10 wt% solution, followed by freezing and lyophilization in a LabConco FreeZone freeze dryer with an external condenser (Medisca, Plattsburgh, NY). The 10 wt% TBA forms a eutectic that inhibits ice crystallization during freezing, preserving the ultrafine structure [8]. Lyophilized samples were cut using a metal blade and exfoliated with adhesive tape, affixed onto an Al pedestal with conductive carbon tape and sputtered with 10 nm Pt, then analyzed by field-emission scanning electron microscopy (FE-SEM) using a JSM-1T710HR microscope (JEOL, Ashland, OR) with an accelerating voltage of 5 kV. Images were collected at 100× and 15,000× magnification and analyzed using ImageJ v.154 [32], using the auto-contrast feature and crosshair grid tool for objective fiber selection (N>100 per sample). Fiber width distributions were collected manually with statistical analysis conducted using OriginPro v.2023b (OriginLab Corp., Northampton, MA).

Particle Size Analysis. Colloidal LHS-1 in pristine or milled forms were dispersed in water (approximately 0.2 g/mL) and characterized with a MRB SYNC (Microtrac, Montgomeryville, PA) at particle loading factors close to 0.1. Milled LHS-1 particles were separated from aqueous slurries by centrifugation and heated to 650 °C for 2 h in air, which removed all organic materials

without sintering the residual powder. Size distributions were obtained for three independent readings, based on particles with >90% sphericity to exclude stray NFC fibers from analysis.

Fabrication of Composite Aerogels. Aqueous slurries of milled LHS-1 and NFC were transferred as 10-mL aliquots into cylindrical molds (20.07 mm i.d.), then stored at –20 °C for 24 h. Frozen aliquots were immersed in 100% ethanol at 20 °C for 24 h, which was repeated five times for complete solvent exchange [33]. The resulting alcogels were loaded into a supercritical dryer (Accudyne Systems, Newark, DE) at 35 °C and 78 bar CO_2 to yield aerogel composite in their final forms.

Characterization of Composite Aerogels. Fourier-transform infrared (FT-IR) spectroscopy was acquired in attenuated total reflection mode using a Nicolet 6700 spectrophotometer (Thermo Scientific, Waltham, MA). Specific surface area (SSA) was measured by Brunauer–Emmett–Teller (BET) analysis with a Tristar 3020 II (Micromeritics, Norcross, GA) using nitrogen adsorption–desorption; aerogel samples were degassed at 80 °C overnight. Aerogel shrinkage (S) was quantified by relative changes in sample diameter according to Equation 1, where d_0 and d_x represent the inner diameter of the cylindrical mold (20.07 mm) and the diameter of the final aerogel sample:

$$S\ (\%) = \frac{d_0 - d_x}{d_0} \times 100\% \quad (1)$$

Bulk density (ρ) was determined according to Equation 2, where m is sample mass (g), d_x is cylinder diameter, and h is cylinder height (cm):

$$\rho = \frac{4m}{\pi {d_x}^2 h} \quad (2)$$

Porosity (P_t) was determined according to Equation 3, where ρ is bulk density (g/cm^3) and ρ_s is the skeletal density as measured by pycnometry with an AccuPyc II 1345 (Micromeritics, Norcross, GA):

$$P_t\ (\%) = \left(1 - \frac{\rho}{\rho_s}\right) \times 100\% \tag{3}$$

Aerogel samples were analyzed in a 10-cm^3 capped cell using helium, with ρ_s based on the mean of 50 trials.

Thermogravimetric analysis (TGA) was conducted on 0.5 g of sample in tared pans using a Q500 TGA instrument (TA Instruments, New Castle, DE) from 25 to 800 °C at a rate of 10 °C/min, under air or nitrogen as specified. Thermal conductivity (k)measurements were performed at 23 °C with a C-Therm Trident instrument (C-Therm Technologies, Fredericton, NB, Canada), using a modified transient plane technique in accord with ASTM D7984 with the modification of having sample thicknesses > 4 mm as required by the instrument.

Mechanical Analysis of Composite Aerogels. Uniaxial compression tests were performed using a Model 5584 electromechanical load frame controlled with Bluehill software (Instron, Norwood, MA), equipped with an SSM sealed S-type load cell (Interface Inc., Scottsdale, AZ) with a calibrated capacity of 2.2 kN (500 lbf) and a reading error below 1%. Cylindrical aerogel specimens were trimmed to obtain flat surfaces prior to loading. Dimensions were measured using an Absolute Digimatic caliper with 0.01 mm resolution (Mitutoyo, Kawasaki, Japan); the mean of three measurements were used to calculate initial cross-sectional area A_0 and initial height h_0.

Compression tests were conducted at 23 °C and a nominal engineering strain rate of $\dot{\epsilon} \approx 2 \times 10^{-3}\ \mathrm{s}^{-1}$, achieved by a constant crosshead displacement rate of 1.27 mm/min (0.05 in/min), corresponding with an initial specimen height (h_0) of 10.6 mm. Force (F) and displacement (d) were recorded at 500 Hz throughout the test, which was terminated at a force of 2.0 kN (450 lbf).

Engineering stress (σ) and strain (ε) were determined according to Eq. 4, where A_0 is the cross-sectional area and Δh is the decrease in specimen height from the crosshead displacement:

$$\sigma = \frac{F}{A_0} = \frac{4F}{\pi d^2}, \qquad \epsilon = \frac{\Delta h}{h_0} = \frac{h_0 - h}{h_0} \tag{4}$$

Compressive stress and strain were reported as positive values, with uncertainty quantified by including four replicate specimens in the analysis. The Young's modulus was determined from the linear elastic region of the stress–strain curve, after applying a seating preload and removing the toe region. The same fitting procedure was applied consistently across replicate specimens.

Statistical Design of Experiments (DOE). Experimental conditions were formulated and analyzed using Design Expert v.13 (Stat-Ease, Inc., Minneapolis, MN). Aerogel samples were prepared from milled aqueous slurries containing NFC, LHS-1, and a variable number of YSZ media. The response surface methodology (RSM) employed a central composite design with one point run in quadruplicate to estimate experimental error (18 formulations in total). Quadratic RSM models were fit by least-squares regression including interaction terms, and plotted as 3D contour surfaces parameterized by the mass fraction of cellulose in aqueous slurry (1–9 w/w%), LHS-1 in aerogel (25–75 wt%), and YSZ media amount (6–12 cylinders).

Predictions for multi-response optimization were transformed using Derringer–Suich functions for each target property, and aggregated using a weighted geometric mean to yield overall desirability. Numerical optimizations were applied toward combinations of desirable outcomes (low ρ, S, k; high P_t, SSA, M) to maximize overall desirability, with the option of applying constraints to input factor ranges and weighting factors (1–10) to modify the steepness of response functions. The importance of key responses could also be weighted (1–5) toward a desired functional outcome, which establishes trade-off priorities and enables optimization algorithms to be guided toward target values when responses conflict during optimization.

RESULTS AND DISCUSSION

Fibrillation of Cellulose Microfibers with LHS-1. Initial studies were aimed at validating the generation of NFC from cellulose products by mineral-assisted grinding, and establishing base conditions for an efficient and practical milling process [34]. Shredded filter paper was used as a model cellulose feedstock for NFC production. Samples were wet milled with and without LHS-1 using YSZ media (1-cm spheres) and characterized by FT-IR and also by FE-SEM at two magnifications to quantify fiber width distributions. IR analysis of dry NFC–LHS composite indicates a broad OH stretch as expected, without additional peaks that might be attributed to chemical modification of cellulose caused by milling (Figure S8). SEM analysis of pristine CMF yielded widths between 3 and 20 μm (**Figure 2a**), whereas pulp milled with YSZ media experienced a decrease in fiber width distribution to the low micron range (**Figure 2b**) and pulp milled with YSZ media and LHS-1 yielded mostly NFC with submicron widths (**Figure 2c**). The log-normal distribution for mineral-ground cellulose indicates a mode fiber width of 0.1 μm, eightfold lower relative to that milled with YSZ media alone (**Figure 2d**). We note that quantitative fiber width analysis was performed with unwashed samples of NFC (**Figure S1**), as extensive washing to remove LHS-1 skewed the outcome by causing significant bundling and loss of finer fibers (**Figure S2**). We further note the importance of wet milling, as control samples milled with LHS-1 but without water did not produce sizable reductions in fiber width. Hydration enables CMF swelling and weakens hydrogen bonding between fibers [9], facilitating their fibrillation by the milling media (**Figure 1**).

To evaluate the impact of milling on LHS-1, particle size analysis was performed after 0, 1, and 2 hours of planetary milling. Samples were pyrolyzed to remove the cellulose prior to particle analysis, which revealed a bimodal distribution in comminution as milling time increased (**Figure**

3). The number fraction of particles < 50 µm (peak at 18.5 µm) was more than 80% after 1 hour and nearly 95% after 2 hours, corresponding with reductions in D50 to 176.2 µm and 124.6 µm, respectively. A reduction in particle size leads to higher surface-to-volume ratios and greater surface energies that favor the formation of stable gels and aerogels [35]. Similarly, reducing the width of fibers embedded in sol-gels and aerogels increases surface contact and bonding at the organic–inorganic interface [36]. The simultaneous comminution of LHS-1 and fibrillation of recycled cellulose can thus be expected to promote the formation of composite aerogels.

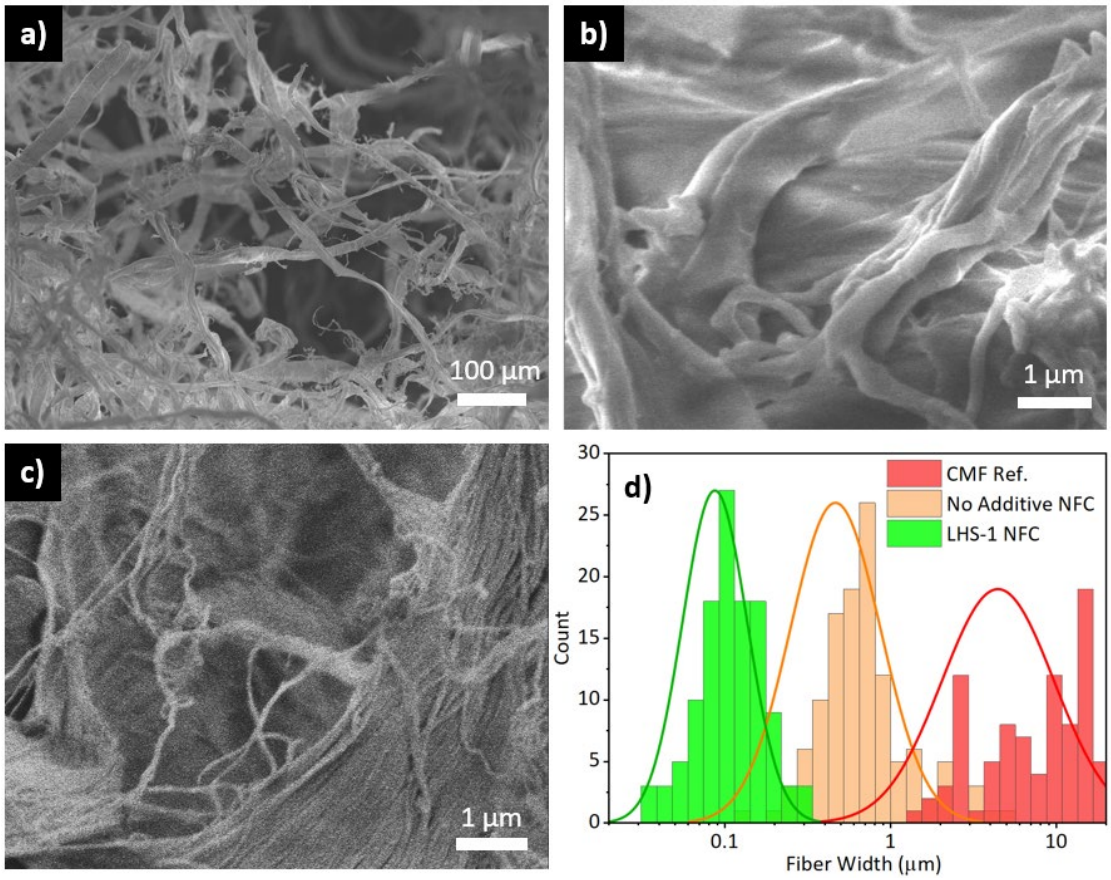


Figure 2. FE-SEM images of cellulose fibers as a function of wet-milling conditions (magnification in parenthesis): (a) Unmilled fibers (100×); (b) fibers milled with YSZ media only (15,000×); (c) fibers milled with YSZ media and LHS-1 (15,000×). (d) Log-normal distribution of cellulose fiber widths with curve fits (see Figure S1 for original image data).

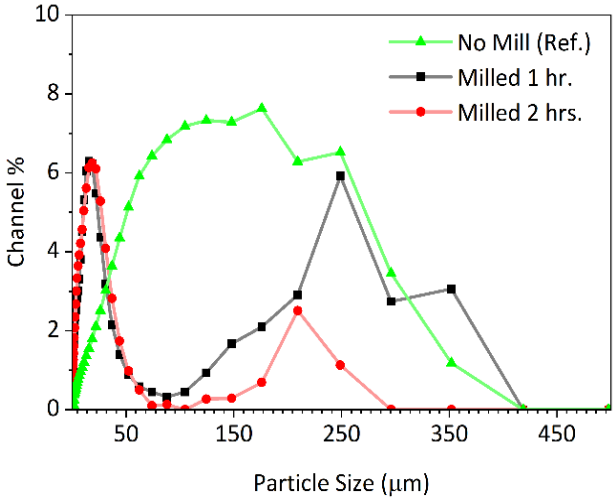


Figure 3. Particle size distributions of LHS-1 from milled samples at different milling times.

Processing Parameters for Composite Aerogel Production. Conditions for converting cellulose and LHS-1 into nanocomposite aerogels were evaluated initially as a function of mill configuration (planetary versus rotary) and type of YSZ media (1-mm or 1-cm spheres, or 1-cm cylinders) at a constant mass ratio of CMF, LHS-1, water, and media. Planetary ball milling provides more kinetic energy and is presumed necessary for applications in low-gravity environments [37], but the choice of grinding media must be established empirically [38]. Visual inspection of the slurries after 2 hours of mixing indicated that planetary milling with 1-cm cylinders produced the most homogeneous suspension, followed by milling with 1-mm spheres (**Figure S3**). Milled slurries were transferred into cylindrical molds and subjected to freezing and SCD to produce aerogels; those prepared by planetary milling produced well-shaped ingots, whereas those prepared by rotary milling were malformed. FE-SEM images of slices from aerogel samples confirmed the greater efficiency of cellulose fibrillation by planetary milling (**Figure S4**). Longer milling times did not provide any benefit: aerogels produced from a cellulose–LHS-1 slurry milled for 4 hours exhibited lower porosity and greater shrinkage than one milled for 2

hours, suggesting a breakdown in NFC fibers over time [9]. We thus proceeded with planetary milling using 1-cm cylinders and 2-h run times for process optimization.

Table 1. Thermal and mechanical properties of NFC/LHS-1 composite aerogels.

Run #	Formulation parameters				Measured Properties					
	NFC (w/w%)[a]	LHS-1 (w/w%)[a]	LHS-1 (wt%)[b]	YSZ media (no.)	Density (ρ, g/cm³)	Porosity (P_t, %)	Shrinkage (S, %)	Specific surface area (SSA, m^2/g)	Thermal conductivity (k, mW/m·K)	Modulus (M, MPa)
1	5	5	50	9	0.172	91.7	18.2	47.7	38.6	1.2
2	1	3	75	6	0.140	95.5	33.5	31.0	34.8	0.025
3	5	5	50	6	0.152	92.6	14.9	56.9	39.1	0.75
4[c]	5	5	50	9	0.169	91.3	18.4	59.8	38.5	0.82
5	1	3	75	12	0.226	95.6	52.0	28.7	N/A[d]	0.012
6	9	3	25	6	0.116	94.2	6.6	47.7	37.4	1.3
7	9	27	75	12	0.484	79.3	24.6	24.6	42.3	2.88
8	1	0.33	25	6	0.049	98.6	36.5	51.0	30.9	0.23
9	1	0.33	25	12	0.078	98.1	44.2	49.0	N/A[d]	0.17
10	9	3	25	12	0.171	91.8	8.9	38.3	35.3	0.49
11	9	9	50	9	0.220	90.1	6.9	40.9	41.4	3.5
12	9	27	75	6	0.457	81.1	3.2	19.0	45.1	1.8
13	5	1.67	25	9	0.123	95.3	20.8	65.8	38.7	1.14
14	1	1	50	9	0.135	96.8	48.2	46.2	N/A[d]	0.14
15	5	5	50	12	0.197	92.3	25.4	53.9	35.4	0.29
16[c]	5	5	50	9	0.169	92.7	16.8	52.8	38.0	0.39
17[c]	5	5	50	9	0.166	93.4	18.6	62.5	38.9	1.77
18	5	15	75	9	0.333	86.2	16.3	34.0	42.5	1.79
19[e]	4.3	0.14	25	6	0.116	94.7	18.5	30.3	30.8	0.49
20[e]	1.0	0.33	25	12	0.072	97.1	40.9	18.9	31.4	0.10
21[e]	1.1	0.70	61.2	12	0.156	95.5	50.6	17.6	30.5	N/A[d]

[a] Initial mass ratio in aqueous slurry prior to planetary milling (2 h) and SCD. [b] Relative mass of LHS-1 in composite aerogel. [c] Replicate of Run 1. [d] Did not meet testing standards. [e] Performed according to DOE optimization (Table 2). Run 19: balanced multi-response; Run 20: weighted for thermal insulation; Run 21: constrained by >60 wt% LHS-1.

Additional variables were evaluated via a design of experiments (DOE) approach by using cellulose in slurry (w/w%), number of YSZ cylinders, and relative mass of LHS-1 in composite (wt%) as process factors, with correlation to aerogel properties (**Table 1**). Milling runs performed with variable loads of recycled cellulose, LHS-1, and YSZ cylinders in aqueous slurries produced aerogels with densities (ρ), porosities (P_t), and shrinkages (S) in the ranges of 0.049–0.484 g/cm^3, 79.3–98.6%, and 3.2–52.0% respectively. Measurement uncertainties based on standard deviations (SD) of replicate samples (N=4) were 0.021 g/cm^3 for ρ, 1.1% for P_t, and 2.9% for S. In addition to these quantitative trends, aerogels produced from slurries with higher solute content (especially NFC w/w%) were more capable of retaining mold geometry (**Figure 4**). Lastly, SEM analysis of milled slurries confirmed the fibrillation of CMF pulp into NFC (**Figures 4d** and **S5**).

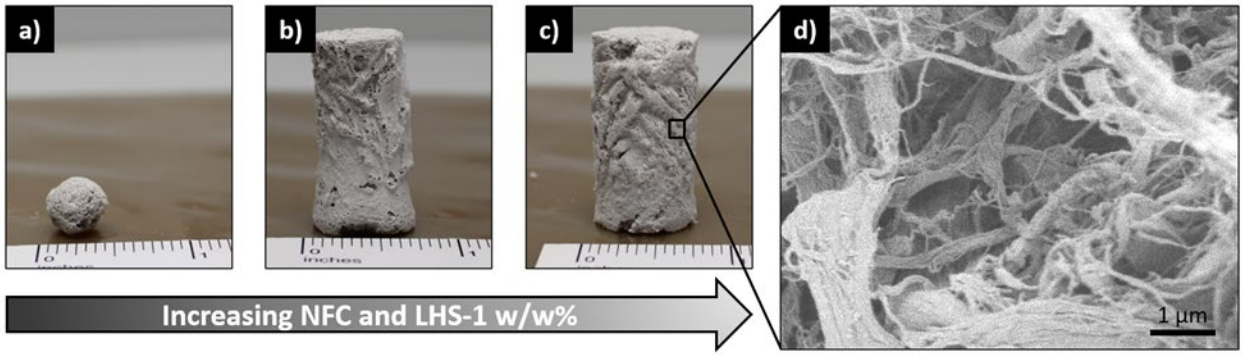


Figure 4. Shape retention of composite aerogels as a function of NFC and total solids in slurry (w/w%). (a) Run 14 (1% NFC, 2% solids); (b) Run 1 (5% NFC, 10% solids); (c) Run 11 (9% NFC, 18% solids) with (d) FE-SEM image at 22,000× magnification.

Multivariate trends based on NFC (w/w% in slurry), LHS-1 (wt% composite), and number of YSZ cylinders during milling can be visualized using empirical model plots with parametric planes (**Figure 5**). The density and porosity plots trend in opposite directions as expected, with decreasing NFC w/w% causing a reduction in aerogel density and an increase in material porosity. This is in

accord with reported trends in the densities and porosities of cellulose-based aerogels based on initial fiber content in the slurry [39]. The 3D plots also confirm that higher LHS-1 wt% increases the density of composite aerogels with a commensurate reduction in porosity (**Figure 5a,b**), however no correlation with sample shrinkage is observed. Instead, shrinkage is strongly affected by cellulose content and is sharply reduced with higher NFC w/w% (**Figure 5c**). Higher ρ, lower P_t, and lower S also correlate with total solute (w/w%) in the slurry (**Figure S6a–c**) [29,39], but the outsized impact of NFC w/w% on shrinkage is noteworthy. Cellulose fibers are widely used to reduce shrinkage in concrete and cement and provide structural reinforcement through nonspecific hydrogen bonding interactions [40,41], and can also reduce the shrinkage of composite aerogels at low loadings [42,43]. The loss of shape retention may also be due in part to the compaction of suspended solids by ice crystals formed during the freezing step, which is well known to degrade the quality of monolithic cellulose aerogels [8]. Lastly, the amount of YSZ media influenced outcomes to a certain extent with the number of cylinders correlating with higher ρ, greater S, and a slight decrease in P_t, again suggesting cellulose fiber degradation with increased milling [9].

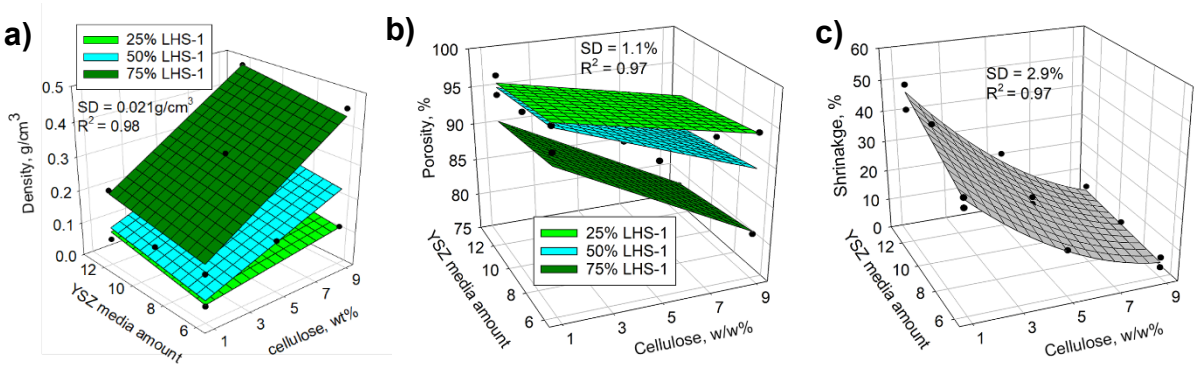


Figure 5. Empirical model plots of aerogel qualities as functions of cellulose content (w/w% slurry), LHS-1 (wt% aerogel), and amount of YSZ media: (a) density (ρ); (b) porosity (P_t); (c) shrinkage (S).

Multivariate parameterization was also conducted for specific surface area (SSA = 19.0–97.6 m^2/g; SD = 4.5 m^2/g), with an apparent maximum at 5 w/w% NFC (**Figure 6a**). The SSAs of LHS-1 derived aerogels are not as high as those produced from silica or fully organic materials [1,33–36,42–44], but nevertheless are improved by the fibrillation of cellulose into NFC. Pore size–volume distribution analysis of select composite aerogels indicates that the samples with highest SSA have a significant population of pores under 5 nm (relative peak at 4 nm), with median pore sizes between 14 and 25 nm (**Figures 6b** and **S7**). The pore dimensions are much smaller than those of NFC and LHS-1 particles (**Figure 2**), however SSA is highest at 5 w/w% cellulose which suggests that nanofibrillation is most effective at this concentration. High SSA is also favored at low aerogel densities and low mineral loadings, implying that NFC is less compacted at 25 wt% LHS-1 than at 75 wt%.

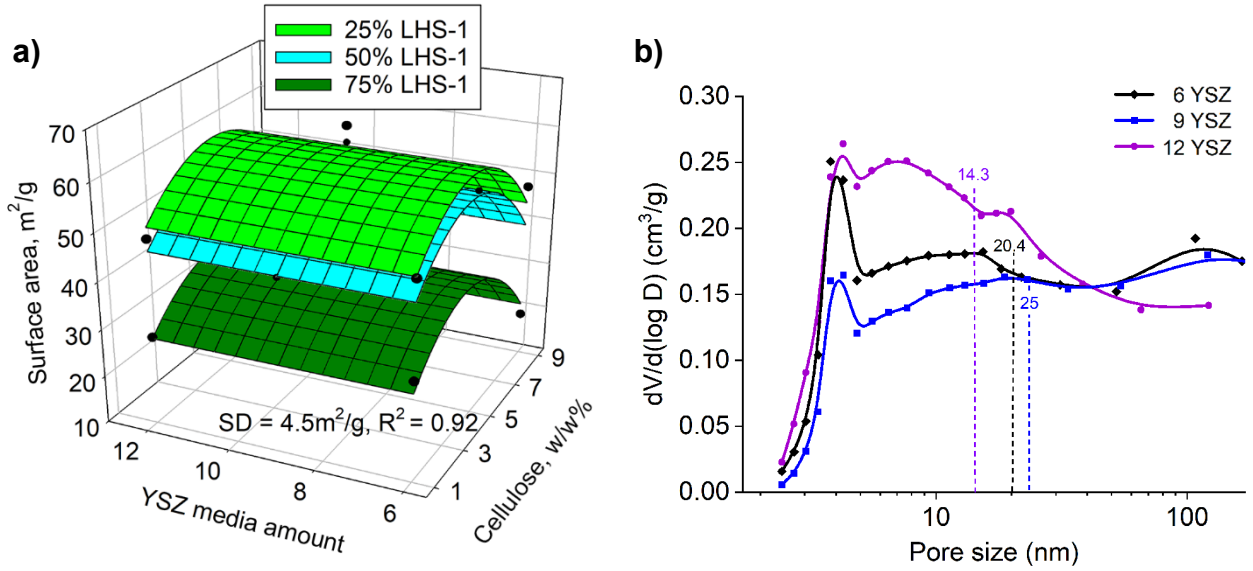


Figure 6. (a) Empirical model plot of specific surface area (SSA) for composite aerogels as functions of cellulose (w/w% slurry) and LHS-1 (wt% aerogel); (b) pore size–volume distribution plots for aerogels produced from 5 w/w% NFC and 50 wt% LHS-1 using different amounts of YSZ media (runs 3, 1, and 15); median pore diameters ($D_{V,50}$) denoted by vertical lines.

Thermal properties of NFC–LHS-1 aerogels. All composite aerogels demonstrate low thermal conductivities (k) between 30 and 45 mW/m·K (SD = 0.7 mW/m·K), with the best (lowest) values correlating with low NFC w/w% and total solute w/w% (**Figures 7** and **S6d**). Further decreases in k are expected in a lunar environment, as the void space within aerogels would be occupied by mostly vacuum rather than air. This has already been demonstrated with several aerogels developed for aerospace applications [44,45], for which thermal conductivity at standard pressure drops severalfold at 0.01 torr. Thermal insulation also correlates strongly with low ρ and high P_t which favor a low LHS-1 wt% (**Figure 6a,b**), however low k is still possible with a high mass ratio of LHS-1 to NFC, which is desirable from an ISRU perspective. As will be discussed below, DOE can optimize parameters to produce aerogels with a favorable balance between thermal insulation and compressive strength.

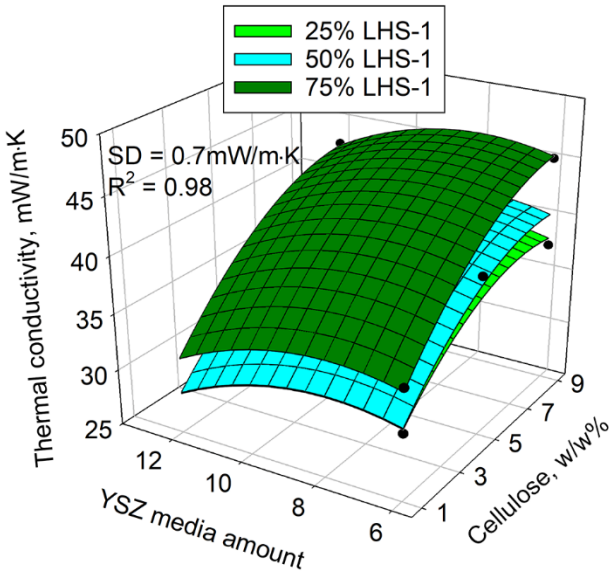


Figure 7. Empirical model plot of thermal conductivity (k) for composite aerogels as functions of cellulose (w/w% slurry), LHS-1 (wt% aerogel), and amount of YSZ media.

One practical consideration in the aerogel's use as a heat shield is its thermal stability. Temperatures on the lunar surface can reach up to 130 °C [46], which is problematic for many

types of organic materials used in aerogel production. To determine the capacity of NFC–LHS-1 aerogels to withstand high temperatures, thermogravimetric analysis (TGA) was performed on a composite sample (**Figure 8**). The onset and endset temperatures for the NFC/LHS-1 aerogel in N_2 were at 345 and 381 °C respectively, whereas those of a reference CMF sample were at 328 and 374 °C, indicating no substantial change in degradation temperatures without LHS-1. This shows that mechanical ball milling and SCD have little effect on the thermal stability of cellulose fibers and nanostructures, although other extrinsic factors can be more significant [47,48].

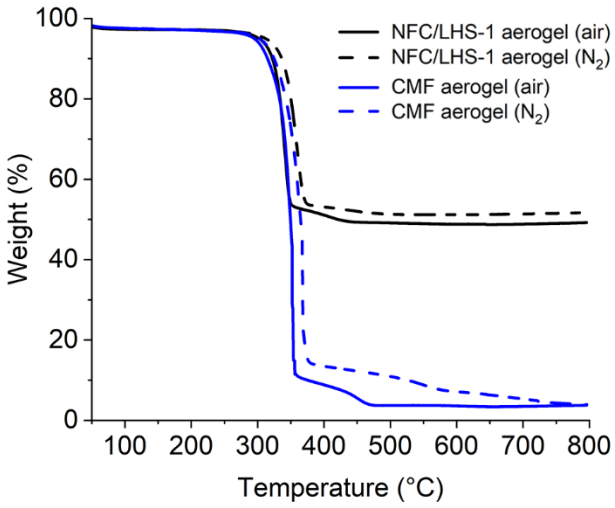


Figure 8. TGA curves of CMF and composite aerogel (5 w/w% NFC, 50 wt% LHS-1).

Mechanical Response of Composite Aerogels. Regolith is a logical feedstock for producing geopolymers in the construction of lunar habitats and other infrastructure [24]. While aerogels are not intended to serve as load-bearing materials, they must still withstand threshold levels of mechanical stress for practical applications. Nanocellulose fibers are already appreciated for their ability to enhance the mechanical properties of composites with high inorganic content, including aerogels [34,49]. In this work, the fibrillation of recycled CMF increases its contact area with ground LHS-1 for better transmission of its mechanical stiffness to the composite aerogel network.

NFC–LHS-1 aerogels were subject to mechanical testing under compression and evaluated according to their Young's modulus, *M* (**Figure 9a**). These were determined from a linear fit to the elastic region of the compressive strain–stress curve, with *M* ranging between 12 kPa and 3.5 MPa (log (SD) = 0.23; **Table 1**). Most of these moduli are considerably higher than those measured for monolithic cellulose aerogels, which typically do not exceed 40 kPa [50]. An empirical model plot indicates that log *M* is sensitive to NFC content (**Figure 9b**), with the highest values correlating with total solids and moderate milling (9 YSZ cylinders) in the initial slurry.

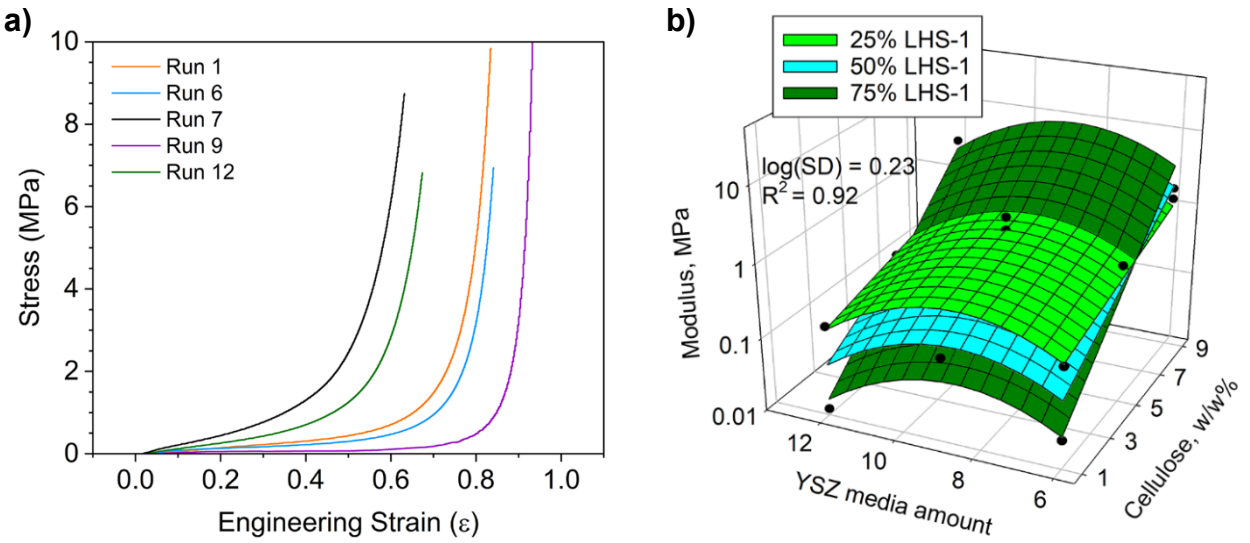


Figure 9. (a) Select compressive stress–strain curves for NFC/LHS-1 composite aerogels (run details listed in Table 1); (b) empirical model plot of compressive modulus (log *M*) as functions of cellulose (w/w% slurry), LHS-1 (wt% aerogel), and amount of YSZ media.

Criteria for Process Optimization. DOE is most meaningful when the responsive surface methodology (RSM) is guided by mission-defined priorities. For example, thermal conductivity and compressive strength correlate similarly with formulation parameters, but their desirable outcomes lie in opposite directions. Tradeoffs can be determined by assigning RSM weighting factors (WFs) to the properties of highest relevance. Optimizations can also be constrained by

ISRU considerations in favor of high LHS-1 content, which can still yield composite aerogels with relatively low thermal conductivities (**Figure 9b**). In this section we consider three scenarios (**Table 2**): (i) multi-response optimization with equal weighting across all six properties; (ii) prioritization of low thermal conductivity (k) with high modulus and low density as secondary objectives; and (iii) optimization of low k constrained by high LHS-1 wt%, with the latter serving as an ISRU factor.

Table 2. DOE optimization of NFC/LHS-1 aerogel properties. [a]

Property (and desired outcome)	**Range of Values**[b]	**Multi-response**		**Thermal Insulation**[c]		**Insulation with ISRU constraint**[c,d]	
		WF / IF	prediction	WF / IF	prediction	WF / IF	prediction
Thermal conduction (low k)	30.9–45.1	1 / 3	36.5	10 / 5	28.6	10 / 5	29.9
Modulus (high M)	0.012–3.50[e]	1 / 3	0.510	1 / 3	0.170	--	0.037
Density (low ρ)	0.078–0.484	1 / 3	0.078	1 / 3	0.101	--	0.153
Porosity (high P_t %)	79.3–98.6	1 / 3	95.2	--	98.1	--	97.0
Shape (low S%)	3.2–52.0	1 / 3	17.5	--	49.7	--	48.9
Surface area (high SSA)	19.0–65.8	1 / 3	60.9	--	51.3	--	40.5
Formulation Parameter	full range (FR)	goal set		goal set		goal set	
NFC (w/w% slurry)	1–9	FR	4.3	FR	1.0	FR	1.1
LHS-1 (wt% solid)	25–75	FR	25.0	FR	25.0	60–75	61.2
YSZ media (amount)	6–12	FR	6	FR	12	FR	12

[a] Overall desirability based on geometric mean of scaled predictive responses with weighting factors (WF) and importance factors (IF); full range (FR) of input factors used in parameterization unless otherwise stated. [b] Property values from Table 1. [c] Unweighted properties not used in optimization and reported as passive responses. [d] Single-objective RSM bounded by high LHS-1 wt%. [e] Log M values used for RSM models.

In the classic multi-response approach, low k is pitted against high M and low S% which favor high cellulose (NFC) loading, whereas low density (ρ), high porosity (P_t), and high SSA favor low LHS-1. Properties are less affected by YSZ media amount, although some are favored by reduced milling action. This yields an optimum formulation of 4.3 w/w% NFC, 25 wt% LHS-1, and 6 YSZ media, with predictions of medium values for k, M, and S%, a low value for ρ, and a high value for P_t. For a RSM focused on lightweight insulation with an emphasis on low thermal conductivity,

a large WF and high importance can be assigned to *k* with smaller values for ρ and *M*. This changes the optimum formulation to 1.0 w/w% NFC, 25 wt% LHS-1, and 12 YSZ media, with predictions of low *k* and ρ as expected but a significant reduction in *M* as well as high *S*%. Both scenarios use 25 wt% LHS-1, which is suboptimal from the ISRU perspective as LHS-1 is far more abundant than recycled cellulose obtained from waste sources. This can be addressed by a single-objective RSM focused on low *k* but constrained by high LHS-1 wt%, which yields an optimized formulation of 1.13 w/w% NFC, 61.2 wt% LHS-1, and 12 YSZ media. In this third case, *k* remains low but at the expense of poor mechanical strength and a higher density.

These predictions were tested by preparing composite aerogels based on each DOE-optimized formulation: For samples with importance biased toward thermal insulation (Runs 20 and 21, **Table 1**), low *k* was indeed achieved (30.5–31.4 mW/m·K) but accompanied by low moduli and high shrinkage as expected. The aerogel based on multi-response optimization had a much higher *M* and lower *S*% (Run 19, **Table 1**), however k and ρ were modestly out of range (30.8 mW/m·K and 11.6 g/cm^3 respectively). We attribute this to the use of a different supercritical dryer in sample preparation

In summary, DOE models can be used to identify acceptable tradeoffs between desirable properties and can also reveal which properties might benefit more from changes in materials chemistry rather than by adjustments in formulation. With respect to thermally insulative aerogels with low NFC w/w%, the elastic moduli of composites may be improved by adding crosslinkers, which are known to yield substantial increases in mechanical strength [51].

Considerations for Extraterrestrial Sustainability. As interest in lunar exploration and colonization continues to grow, so too does the need for efficient usage of limited resources in

outer space. Sustainable practices in space exploration are still at the primordial stage: for example, extraterrestrial waste on the International Space Station is typically jettisoned, contributing to cislunar debris and low-Earth orbit clutter [52]. Some systems have been developed to convert solid waste into fuel [16], however the scarcity of organic matter in space underscores the importance of salvaging materials for ISRU upcycling. Producing composite aerogels with NFC and colloidal LHS-1 aligns well with this approach: cellulose recycled from waste feedstocks can be fibrillated with local regolith by a low-energy ball-milling process, and the composites can be converted readily into lightweight aerogels for thermal insulation. Such efforts are currently underway in our laboratory and will be reported in due course. NFC–regolith composites can also be tailored for diverse needs: aerogels with high porosity and SSA can serve as air filters for dust mitigation [53], whereas denser, mechanically robust composites can function as lightweight structures for packaging or furniture applications [34,54].

CONCLUSIONS

We have designed an ISRU-based approach to composite aerogels that can be implemented with feedstocks based on recycled cellulose with local regolith, with application toward thermal insulation for lunar habitats. Cellulose fibers can be converted into NFC (mode width < 0.1 μm) by two hours of planetary wet-milling using cylindrical YSZ media and colloidal LHS-1, which is also comminuted to micron-sized particles. Slurries of NFC and LHS-1 can be converted into aerogels by supercritical drying and evaluated for multiple properties, including high thermal stability and low conductivity. DOE analysis was performed by preparing samples according to a central composite design parameterized by mass ratios of cellulose in aqueous slurry, LHS-1 in

composite aerogel, and number of YSZ media used, and by estimating property outcomes using least-squares fits. Aerogels prepared with a low cellulose w/w% tended toward low thermal conductivity (k ~30 mW/m·K) and high porosity (>98%), but also experienced shrinkage and a low compressive modulus (M). The impact of regolith on aerogel properties was more nuanced, with high LHS-1 wt% (favored from an ISRU perspective) supporting either low k or high M depending on other factors. This was confirmed by using DOE optimization models to evaluate tradeoffs between k, ρ, and M, which validated the potential of using composite aerogels with a high regolith content for thermal insulation.

Additional developments are needed to enhance the production and performance of cellulose–regolith aerogels as lunar insulation materials. First, producing aerogels by lyophilization (freeze drying) rather than by SCD is far more practical in a lunar environment, with sub-microtorr pressures and dark temperatures well below –100 °C. The ultrafine structure of NFC can be preserved by adding simple cryoprotectants such as alcohols or sugars to suppress the kinetics of ice crystallization [8,55]. Second, comminution of regolith to submicron particles is readily achievable with planetary (centrifugal) milling with increased time or kinetic energy, which can be performed prior to adding recycled cellulose. Third, crosslinkers should be studied as additives that can improve the mechanical strength of cellulose-reinforced composite aerogels at low NFC loading. Lastly, additional regolith compositions should be evaluated as substrates to validate the general utility of NFC–regolith aerogels [56].

ASSOCIATED CONTENT

Supporting Information: FE-SEM images, NFC fiber width analysis, additional correlations between aerogel composition and properties, additional pore size–volume distributions. The

Supporting Information is available free of charge at https://pubs.acs.org/doi/10.1021/XXX. Additional data and calculations will be provided upon request.

ACKNOWLEDGMENTS

This work was funded by The Indiana Space Grant Consortium (INSGC), the National Science Foundation (CHE-2204206), and Purdue University. J.S. also thanks the NASA OSTEM internship program and for funding and support.

ABBREVIATIONS

CMF, cellulose microfibers; D50, median particle diameter; $D_{V,50}$, median diameter at 50% volume distribution; DOE, design of experiments; FE-SEM, field-emission scanning electron microscopy; FR, full range; IF, importance factor; ISRU, in-situ resource utilization; k, thermal conductivity; lbf, pound-force; LHS, lunar highland simulant; M, elastic modulus; NFC, nanofibrillated cellulose; P_t, porosity; ρ, density; RSM, response surface methodology; S, shrinkage; SCD, supercritical drying; SD: standard deviation; SSA, specific surface area; TBA, *tert*-butyl alcohol; TGA, thermogravimetric analysis; WF, weighting factor; w/w%, mass ratio in liquid slurry; wt%, mass ratio in aerogel; YSZ, yttria-stabilized zirconia.

AUTHOR CONTRIBUTIONS

J.S.: Data curation, Investigation, Methodology, Writing – original draft. J.M.: Data curation. A.H.: Data curation. D.A.S.: Data curation. J.L.S.: Investigation, Writing – editing. A.T.: Data curation, Methodology, Writing – editing. H.G.: Conceptualization, Project administration, Data curation, Resources, Supervision, Writing – review and editing. A.W.: Conceptualization, Project administration, Data curation, Resources, Supervision, Writing – review and editing.

Notes

The authors declare no competing financial interests.

AUTHOR INFORMATION

Corresponding Authors

Alexander Wei– Tarpo Department of Chemistry, Purdue University, 560 Oval Drive, West Lafayette, Indiana 47907, USA; School of Materials Engineering, Purdue University, 701 W. Stadium Avenue, West Lafayette, Indiana 47907, USA; https://orcid.org/0000-0002-8587-1037; Email: alexwei@purdue.edu

Haiquan Guo– Universities Space Research Association, Cleveland, OH 44135, USA; https://orcid.org/0000-0002-9706-9447; Email: haiquan.n.guo@nasa.gov

Authors

Jacob Staker– Tarpo Department of Chemistry, Purdue University, 560 Oval Drive, West Lafayette, Indiana 47907, USA; https://orcid.org/0009-0004-7594-4978.

Janice Mather– University of Akron, Akron, OH 44325, USA.

Annabelle Hegeman– University of Akron, Akron, OH 44325, USA.

Daniel A. Scheiman– Universities Space Research Association, Cleveland, OH 44135, USA; https://orcid.org/0000-0001-5252-7363.

Jamesa L. Stokes– NASA Glenn Research Center, Cleveland, OH 44135, USA; https://orcid.org/0000-0002-0675-9988.

Andres Tovar– School of Mechanical Engineering, Purdue University, Indianapolis, IN 46202, USA; https://orcid.org/0000-0003-2727-6587.

REFERENCES

1. Long, L.; Weng, Y.; Wang, Y. Cellulose aerogels: Synthesis, applications and prospects. *Polymers*, **2018**, *10*, 623, DOI: 10.3390/polym10060623.

2. Sharma, C; Sharma, S. N.; Srivastava, R. Analysis of cellulose extracted from waste products. *Coll. Polym. Sci.* **2022**, *300*, 1027–1036, DOI: 10.1007/s00396-022-05005-w.

3. Magalhaes, S.; Fernandes, C.; Pedrosa, J. F. S.; Alves, L.; Medronho, B.; Ferreia, P. J. T.; Rasteiro, M. d. G. Eco-friendly methods for extraction and modification of cellulose: An overview. *Polymers* **2023**, *14*, 3138, DOI: 10.3390/polym15143138.

4. Kumar, V.; Pathak, P.; Bharadwaj, N. J. Waste paper: An underutilized but promising source for nanocellulose mining. *Waste Manag*. **2020**, *102*, 281–303, DOI: 10.1016/j.wasman.2019.10.041.

5. Zhang, Z.; Kong, Y.; Gao, J.; Han, X.; Lian, Z.; Liu, J.; Wang, W.; Yang, X. Engineering strong man-made cellulosic fibers: A review of the wet spinning process based on cellulose nanofibrils. *Nanoscale* **2024**, *16*, 6383–6401, DOI: 10.1039/D3NR06126D.

6. (a) Thomas, B.; Raj, M. C.; Athira, K. B.; Rubiyah, M. H.; Joy, J.; Moores, A.; Drisko, G. L.; Sanchez, C. Nanocellulose, a Versatile Green Platform: From Biosources to Materials and Their Applications. *Chem. Rev.* **2018**, *118*, 11575-11625, DOI: 10.1021/acs.chemrev.7b00627. (b) Ioelovich, M. J. Microcellulose vs nanocellulose – A review. *World J. Adv. Eng. Technol. Sci.* **2022,** *5*, 001–015, DOI: 10.30574/wjaets.2022.5.2.0037.

7. Nuruddin, M.; Hosur, M.; Uddin, M. J.; David, B.; Shaik, J. A novel approach for extracting cellulose nanofibers from lignocellulosic biomass by ball milling combined with chemical treatment. *J. Appl. Polym. Sci.* **2016**, *133*, 42990*,* DOI: 10.1002/app.42990.

8. Mavlan, M.; Chang, T.; Feng, R.; Wilkinson, J. R.; Nicholas, R. J.; Idahagbon, N. B.; Youngblood, J. P.; Wei, A. Mechanochemical esterification of cellulose nanofibers lyophilized from eutectic water–*tert*-butanol mixtures. *Cellulose* **2023**, *30*, 8805–8817, DOI: 10.1007/s10570-023-05435-x.

9. Piras, C. C.; Fernandez-Prieto, S.; De Borggraeve, W. M. Ball milling: a green technology for the preparation and functionalisation of nanocellulose derivatives. *Nanoscale Adv.* **2019**, *1*, 937–947, DOI: 10.1039/C8NA00238J.

10. Zhao, Q.-Q.; Yamada, S.; Jimbo, G. The mechanism and limit of fineness of a planetary. *KONA Powder Particle J.* **1989**, *7*, 29–36, DOI: 10.14356/kona.1989007.

11. Taylor, L.; Skuse, D.; Blackburn, S.; Greenwood, R. Stirred media mills in the mining industry: Material grindability, energy-size relationships, and operating conditions. *Powder Technol.* **2020**, *369*, 1–16, DOI: 10.1016/j.powtec.2020.04.057.

12. Kumar, A; Sahu, R; Tripathy, S. K. Energy-efficient advanced ultrafine grinding of particles using stirred mills-- A review. *Energies* **2023**, *16*, 5277, DOI: 10.3390/en16145277.

13. Huang, D.; Hong, H.; Huang, W.; Hong, X. Scalable preparation of cellulose nanofibers from office waste paper by an environment-friendly method. *Polymers* **2021**, *13*, 3119, DOI: 10.3399/polym13183119.

14. Gilbert, M. Cellulose plastics. In *Brydson's Plastics Materials*, 8th ed.; Gilbert, M. Ed.; Elsevier, 2017, pp 617–630, DOI: 10.1016/B978-0-323-35824-8.00022-0.

15. Ruiz-Caldas, M.; Carlsson, J.; Sadiktsis, I.; Nilsson, U.; Mathew, A. P. Cellulose nanocrystals from postconsumer cotton and blended fabrics: A study on their properties, chemical composition, and process efficiency. *ACS Sustain. Chem. Eng.* **2022**, *10*, 3787–3798, DOI: 10.1021/acssuschemeng.2c00797.

16. Linne, D. L.; Palaszewski, B. A.; Gokoglu, S.; Balasubramaniam, B.; Hegde, U. G.; Gallo, C. A. Waste management options for long-duration space missions: When to reject, reuse, or recycle. 7th Symposium on Space Resource Utilization, *AIAA SciTech,* **2014**, DOI: 10.2514/6.2014-0497.

17. Lockhart, L. Recycling in space: Waste handling in a microgravity environment. Oct. 10th, 2018. https://www.nasa.gov/missions/station/recycling-in-space-waste-handling-in-a-microgravity-environment-challenge (last accessed March 2, 2026).

18. Pino, P.; Salmeri, A.; Hugo, A.; Hume, S. Waste management for lunar resources activities: Toward a circular lunar economy. *New Space* **2021**, *10*, 274–283, DOI: 10.1089/space.2021.0012.

19. Sanders, G; Kleinhenz, J. Moon to Mars in situ resource utilization (ISRU) status update. International Cooperation Networking for Moon to Mars Resource Exploration and In-Situ Resource Utilization, 2024. https://ntrs.nasa.gov/citations/20240013906 (last accessed March 2, 2026).

20. Lee, S.; Riessen, A. A Review on geopolymer technology for lunar base construction. *Materials* **2022**, *15*, 4516, DOI: 10.3390/ma15134516.

21. Cool, N. I, Perez-Beltran, S.; Cheng, J.; Rivera-Gonzalez, N.; Bronner, D.; Anita; , E.; Zakira, U.; Farahbakhsh, M.; Liu, K.; Hsu, J.; Birgisson, B.; Banerjee, S. Matrix transformation of lunar regolith and its use as a feedstock for additive manufacturing. *iScience* **2023**, *26*, 106382, DOI: 10.1016/j.isci.2023.106382.

22. Zheng, X.; Zhao, C.; Sun, X.; Dong, W. Lunar regolith geopolymer concrete for in-situ construction of lunar bases: A review. *Polymers* **2024**, *16*, 1582, DOI: 10.3390/polym16111582.

23. Sun, Y.; Ma, S.; Chen, Q.; Chen, G.; He, P.; Wang, Y.; Qiu, J.; Jia, D. Lunar regolith simulant-derived 3D-printed geopolymers with optimized mechanical and thermal management properties. *Compos. A: Appl. Sci. Manuf.* **2025**, *196*, 108989, DOI: 10.1016/j.compositesa.2025.108989.

24. McCallum, C.: Liang, Y.; Tushar, N.; Xu, B.; Zhao, B.; Zeng, H.; Shou, W. Additive manufacturing of lunar regolith for reconfigurable building blocks toward lunar habitation. *arXiv* **2025**, DOI: 10.48550/arXiv.2506.06392.

25. Grundstrom, B; Schild, T; Cowley, A. Additive manufacturing of lunar regolith simulant using direct ink writing. *Spool* **2021**, *8*, 55–70, DOI: 10.7480/spool.2021.2.5268.

26. Rosa, I; Coto, A; Allende, M. I; Lepech, M. D.; Loftus, D. J. Designing biopolymer-bound regolith composites for maximum compressive strength. In *Earth and Space 2021*, **2021**; pp. 200–214, DOI: 10.1061/9780784483381.019.

27. Dikshit, R.; Dey, A.; Gupta, N.; Varma; S. C.; Venugopal, I.; Viswanathan, K.; Kumar, A. Space bricks: From LSS to machinable structures via MICP. *Ceram. Int.* **2021**, *47*, 14892–14898, DOI: 10.1016/j.ceramint.2020.07.309.

28. Gupta, N.; Kumar, A.; Viswanathan, K. Biopolymers can be used for consolidation of lunar and Martian regoliths. *Acta Astronaut.* **2026**, *245*, 897–907, DOI: 10.1016/j.actaastro.2026.03.042.

29. Borella, L.; Rozo, A.; Perfetti, C.; Iorio, C. S. Characterization of composite freeze-dried aerogels with simulant lunar regolith for space applications. *Materials* **2023**, *16*, 5797, DOI: 10.3390/ma16175797.

30. Orlovska, I; Podolich, O; Kukharenko, O; Zaets, I; Reva, O; Khiruneko, L; Zmejkoski, D; Togalsky, S.; Barh, D.; Tiwari, S. et al. Bacterial cellulose retains robustness but its synthesis declines after exposure to a Mars-like environment simulated outside the International Space Station. *Astrobiology* **2021**, *21*, 706–717, DOI: 10.1089/ast.2020.2332.

31. Koehle, A. P.; Brumwell, S. L.; Seto, E. P.; Lynch, A. M.; Urbaniak, C. Microbial applications for sustainable space exploration beyond low Earth orbit. *Npj microgravity* **2023**, *9*, 47, DOI: 10.1038/s41526-023-00285-0.

32. Schneider, C. A.; Rasband, W. S.; Eliceiri, K. W. NIH Image to ImageJ: 25 years of image analysis. *Nat. Methods* **2012**, *9*, 671–675, DOI: 10.1038/nmeth.2089.

33. Staker, J.; White, G. M.; Pasilova, S.; Scheiman, D. A.; Guo, H.; Tovar, A.; Siegel, A. P. Mitigating Shrinkage and Enhancing the Structure of Thermally Insulating Starch Aerogel via Solvent Exchange and Chitin Addition. *Macromol* **2025**, *5*, 28, DOI: 10.3390/macromol5020028.

34. Phipps, J., Current and potential use of highly fibrillated cellulose in the paper and board industry. In *Advances in Pulp and Paper Research*, Coffin, D.; Batchelor, W., Eds. Cambridge, 2022; pp 249–268, DOI: 10.15376/frc.2022.1.249.

35. Payanda Konuk, O.; Alsuhile, A. A. A. M.; Yousefzadeh, H.; Ulker, Z.; Bozbag, S. E.; García-González, C. A.; Smirnova, I.; Erkey, C. The effect of synthesis conditions and process parameters on aerogel properties. *Front. Chem.* **2023**, *11*, 1294520, DOI: 10.3389/fchem.2023.1294520.

36. Mazrouei-Sebdani, Z.; Naeimirad, M.; Peterek, S.; et al. Multiple assembly strategies for silica aerogel–fiber combinations– A review. *Mater. Design* **2022**, *223*, 111228, DOI: 10.1016/j.matdes.2022.111228.

37. Ozaki, S.; Ishigami, G.; Otsuki, M.; Miyamoto, H.; Wada, K.; Watanabe, Y.; Nishino, T.; Kojima, H.; Soda, K.; Nakao, Y.; Sutoh, M.; Maeda, T.; Kobayashi, T. Granular flow experiment using artificial gravity generator at International Space Station. *npj Microgravity* **2023**, *9*, 61, DOI: 10.1038/s41526-023-00308-w.

38. Romeis, S.; Schmidt, J.; Peukert, W. Mechanochemical aspects in wet stirred media milling. *Int. J. Miner. Process.* **2016**, *156*, 24–31, DOI: 10.1016/j.minpro.2016.05.018.

39. Lin, W.; Jana, S. C. Analysis of porous structures of cellulose aerogel monoliths and microparticles. *Micropor. Mesopor. Mater.* **2021**, *310*, 110625, DOI: 10.1016/j.micromeso.2020.110625.

40. Haddad Kolour, H.; Ahmed, M.; Alyaseen, E.; Landis, E. N. An Investigation on the Effects of Cellulose Nanofibrils on the Performance of Cement Paste and Concrete. *Adv. Civil Engin. Mater.* **2018**, *7*, 463–478, DOI: 10.1520/acem20180048.

41. Ren, G.; Guo, Y.; Shen, A.; Pan, H.; Wu, H.; Deng, S. Effects of cellulose fiber on shrinkage, anticrack performance, and mechanical properties of concrete. *Construct. Build. Mater.* **2024**, *451*, 138824, DOI: 10.1016/j.conbuildmat.2024.138824.

42. Jaxel, J.; Markevicius, G.; Rigacci, A.; Budtova, T. Thermal superinsulating silica aerogels reinforced with short man-made cellulose fibers. *Compos. A. Appl. Sci. Manuf.* **2017**, *103*, 113–121, DOI: 10.1016/j.compositesa.2017.09.018.

43. Sai, H.; Wang, M.; Miao, C.; Song, Q.; Wang, Y.; Fu, R.; Wang, Y.; Ma, L.; Hao, Y. Robust Silica-Bacterial Cellulose Composite Aerogel Fibers for Thermal Insulation Textile. *Gels* **2021**, *7*, DOI: 10.3390/gels7030145

44. Guo, H.; Cakmak, M; Sprowl, G; et al. Polyimide aerogels cross-linked through amine functionalized polyoligomeric silsesquioxane. *ACS Appl. Mater. Interfaces* **2011**, *3*, 546–552, DOI: 10.1021/am101123h.

45. Szabó, Á.; Lakatos, Á. Thermal analysis of aerogels and their vacuum-formed forms, their potential uses, and their effects on the environment. *Case Stud. Therm. Eng.* **2024**, *56*, 104284, DOI: 10.1016/j.csite.2024.104284.

46. Kessler, P.; Prater, T.; Nickens, T.; Harris, D. In *Artemis Deep Space Habitation: Enabling a Sustained Human Presence on the Moon and Beyond*, *IEEE Aerospace Conference*, **2022**; pp. 1–12, DOI: 10.1109/aero53065.2022.98433933.

47. Phanthong, P.; Guan, G.; Ma, Y.; Hao, X.; Abudula, A. Effect of ball milling on the production of nanocellulose using mild acid hydrolysis method. *J. Taiwan Inst. Chem. Eng.* **2016**, *60*, 617–622, DOI: 10.1016/j.jtice.2015.11.001.

48. D'Acierno, F.; Michal, C. A.; MacLachlan, M. J. Thermal Stability of Cellulose Nanomaterials. *Chem. Rev.* **2023**, *123*, 7295–7325, DOI: 10.1021/acs.chemrev.2c00816.

49. Chen, Y.; Zhang, L.; Yang, Y.; Pang, B.; Xu, W.; Duan, G.; Jiang, S.; Zhang, K. Recent Progress on Nanocellulose Aerogels: Preparation, Modification, Composite Fabrication, Applications. *Adv. Mater.* **2021**, *33*, 2005569, DOI: 10.1002/adma.202005569.

50. Paulauskiene, T.; Sirtaute, E.; Tadzijevas, A.; Uebe, J. Mechanical properties of cellulose aerogel composites with and without crude oil filling. *Gels* **2024**, *10*, 135, DOI: 10.3390/gels10020135.

51. Jiang, S.; Jiang, S.; Yan, J.; Lin, C.; Wang, W.; Jiang, S.; Cao, L.; Guo, R. In situ cross-linking reinforced cellulose aerogel fibers for thermal insulation and multifunctional applications. *Ind. Eng. Chem. Res*. **2024,** *63*, 15301–15313, DOI: 10.1021/acs.iecr.4c02456.

52. Filho, W. L.; Abubakar, I. R.; Hunt, J.D.; Dinis, M. A. P. Managing space debris: Risks, mitigation measures, and sustainability challenges. *Sustain. Fut.* **2025**, *10*, 100849, DOI: 10.1016/j.sftr.2025.100849.

53. Sepahvand, S.; Kargarzadeh, H.; Jonoobi, M.; Ashori, A.; Ismaeilimoghadam, S.; Varghese, R. T.; Chirayl, C. J.; Azimi, B.; Danti, S. Recent developments in nanocellulose-based aerogels

as air filters: A review. *Int. J. Biol. Macromol.* **2023**, *246*, 125721, DOI: 10.1016/j.ijbiomac.2023.125721.

54. Sheng, J.; Zhang, M.; Yang, R.; Xie, W.; Wang, Y. High-Performance Calcium Silicate Board Reinforced by Microfibrillated Cellulose/Microsilica. *ACS Sustain. Chem. Eng.* **2023**, *11*, 7053–7061, DOI: 10.1021/acssuschemeng.3c00099.
55. Deller, R. C.; Vatish, M.; Mitchell, D. A.; Gibson, M. I. Synthetic polymers enable non-vitreous cellular cryopreservation by reducing ice crystal growth during thawing. *Nat. Commun.* **2014**, *5*, 3244, DOI: 10.1038/ncomms4244.
56. Long-Fox, J. M.; Britt, D. T. Characterization of planetary regolith simulants for the research and development of space resource technologies. *Front. Space Technol.* **2023**, *4*, 1255535, DOI: 10.3389/frspt.2023.1255535.
57. Stanciu, M.-C.; Tanasă, F.; Teacă, C.-A. Crystallinity Changes in Modified Cellulose Substrates Evidenced by Spectral and X-Ray Diffraction Data. *Polysaccharides* **2025**, *6*, 30, DOI:10.3390/polysaccharides6020030.